Research Article | Vol. 25, No. 26 | 25 Dec 2017 | OPTICS EXPRESS 33216
Optics EXPRESS

Electronic initiation and optimization of nonlinear polarization evolution mode-locking in a fiber laser

DAVID G. WINTERS,[1,*] MATTHEW S. KIRCHNER,[1] STERLING J. BACKUS,[1,2] AND HENRY C. KAPTEYN[1,3]

[1]*Kapteyn-Murnane Laboratories, Inc., Boulder, Colorado, USA*
[2]*Colorado State University, Fort Collins, Colorado, USA*
[3]*Department of Physics, University of Colorado, Boulder, Colorado, USA*
[*]*dwinters@kmlabs.com*

Abstract: We describe a system for automated modelocking and optimization of a fiber laser oscillator employing nonlinear polarization evolution. Using four liquid crystal variable retarders, we fully control the fiber launch and output polarization states, enabling compensation for mechanical and environmental perturbations to the fiber cavity. We demonstrate mapping of the modelocking regions for an ANDi fiber oscillator and demonstrate that local and global optimization algorithms can be used to maintain the laser in the same operating state. This technique enables robust operation of nonlinear polarization evolution modelocked fiber lasers, rivaling the stability of PM fiber lasers while maintaining the advantages of the NPE modelocking mechanism.

OCIS codes: (140.3510) Lasers, fiber; (140.7090) Ultrafast lasers; (230.3720) Liquid-crystal devices.

References and links

1. L. E. Nelson, D. J. Jones, K. Tamura, H. A. Haus, and E. P. Ippen, "Ultrashort-pulse fiber ring lasers," Appl. Phys. B Lasers Opt. **65**(2), 277–294 (1997).
2. M. Hofer, M. H. Ober, F. Haberl, and M. E. Fermann, "Characterization of ultrashort pulse formation in passively mode-locked fiber lasers," IEEE J. Quantum Electron. **28**(3), 720–728 (1992).
3. S. L. Brunton, X. Fu, and J. N. Kutz, "Self-Tuning Fiber Lasers," IEEE J. Sel. Top. Quantum Electron. **20**(5), 1101408 (2014).
4. S. L. Brunton, X. Fu, and J. N. Kutz, "Extremum-Seeking Control of a Mode-Locked Laser," IEEE J. Quantum Electron. **49**(10), 852–861 (2013).
5. M. Olivier, M.-D. Gagnon, and M. Piché, "Automated mode locking in nonlinear polarization rotation fiber lasers by detection of a discontinuous jump in the polarization state," Opt. Express **23**(5), 6738–6746 (2015).
6. R. I. Woodward and E. J. R. Kelleher, "Towards 'smart lasers': self-optimisation of an ultrafast pulse source using a genetic algorithm," Sci. Rep. **6**(1), 37616 (2016).
7. X. Shen, W. Li, M. Yan, and H. Zeng, "Electronic control of nonlinear-polarization-rotation mode locking in Yb-doped fiber lasers," Opt. Lett. **37**(16), 3426–3428 (2012).
8. U. Andral, J. Buguet, R. Si Fodil, F. Amrani, F. Billard, E. Hertz, and P. Grelu, "Toward an autosetting mode-locked fiber laser cavity," J. Opt. Soc. Am. B **33**(5), 825 (2016).
9. M. Karlsson, J. Brentel, and P. A. Andrekson, "Long-Term Meassurement of PMD and Polarisation Drift in Installed Fibers," J. Lightwave Technol. **18**(7), 941–951 (2000).
10. D. Radnatarov, S. Khripunov, S. Kobtsev, A. Ivanenko, and S. Kukarin, "Automatic electronic-controlled mode locking self-start in fibre lasers with non-linear polarisation evolution," Opt. Express **21**(18), 20626–20631 (2013).
11. Z. Zhuang, S. W. Suh, and J. S. Patel, "Polarization controller using nematic liquid crystals," Opt. Lett. **24**(10), 694–696 (1999).
12. M. Nikodem, K. Krzempek, K. Zygadlo, G. Dudzik, A. Waz, K. Abramski, and K. Komorowska, "Intracavity polarization control in mode-locked Er-doped fibre lasers using liquid crystals," Opto-Electron. Rev. **22**(2), 113–117 (2014).
13. U. Andral, R. S. Fodil, F. Amrani, F. Billard, E. Hertz, and P. Grelu, "Fiber laser mode locked through an evolutionary algorithm," Optica **2**(4), 275–278 (2015).
14. A. Chong, J. Buckley, W. Renninger, and F. Wise, "All-normal-dispersion femtosecond fiber laser," Opt. Express **14**(21), 10095–10100 (2006).
15. K. Kieu and F. W. Wise, "All-fiber normal-dispersion femtosecond laser," Opt. Express **16**(15), 11453–11458 (2008).

#308632 https://doi.org/10.1364/OE.25.033216
Journal © 2017 Received 6 Oct 2017; revised 13 Dec 2017; accepted 14 Dec 2017; published 21 Dec 2017

Optics EXPRESS

16. B. G. Bale, J. N. Kutz, A. Chong, W. H. Renninger, and F. W. Wise, "Spectral filtering for high-energy mode-locking in normal dispersion fiber lasers," J. Opt. Soc. Am. B **25**(10), 1763–1770 (2008).
17. A. Chong, W. H. Renninger, and F. W. Wise, "Properties of normal-dispersion femtosecond fiber lasers," J. Opt. Soc. Am. B **25**(2), 140–148 (2008).
18. J. L. Devore, *Probability and Statistics for Engineering and the Sciences* (Brooks/Cole, 2012).
19. S. Kirkpatrick, C. D. Gelatt, Jr., and M. P. Vecchi, "Optimization by Simulated Annealing," Science **220**(4598), 671–680 (1983).
20. G. Dueck and T. Scheuer, "Threshold accepting: A general purpose optimization algorithm appearing superior to simulated annealing," J. Comput. Phys. **90**(1), 161–175 (1990).
21. P. Charbonneau, "An Introduction to Genetic Algorithms for Numerical Optimization," NCAR Technical Note TN-450 + IA (2002).

1. Introduction

Nonlinear polarization evolution (NPE) is an established method for inducing modelocking in a laser. In NPE, the polarization state of a beam within the laser cavity can change in an intensity-dependent way through interaction with a material. When combined with a polarizer, this nonlinear polarization rotation can be configured as a saturable absorber, where a decrease in optical loss within a laser cavity with increasing intensity is used to encourage pulse formation (modelocked operation) in laser oscillators [1,2]. The NPE mechanism is particularly flexible in that it is intrinsically fast and broad bandwidth, facilitating the shortest possible pulse duration, and is robust against damage or long-term materials degradation.

To achieve the desired saturable-loss behavior, the polarization of the light into the nonlinear medium must be controlled. This is typically implemented using one or more fixed retarders (wave plates or fiber loops) that can be rotated to achieve the desired polarization state. Motorized rotation stages have been proposed [3,4] and demonstrated [5,6] to automatically identify the correct configuration for modelocking. Alternately, polarization control can be implemented by applying force to the fiber to control stress-induced birefringence in the fiber [7]. It has also been demonstrated that thermal-induced birefringence polarization controllers can be used for automatic modelocking [8]. However, motorized elements and those which rely on thermal effects can be slow, requiring significant time to automatically modelock the laser. Applying force to a fiber using (for example) a piezoelectric actuator can be fast, but requires high voltages to drive the actuator, and the force required for a given polarization may drift over time, requiring additional compensation.

The NPE modelocking mechanism is particularly well suited for fiber lasers, where propagation in a guided mode allows for accumulation of nonlinear phase. This rotation happens primarily near the end of the fiber cavity, after the pulse has gone through the gain fiber. Since the transfer function of the fiber is not known, the correct input polarization state cannot be known a-priori. Also, the polarization state of light inside an optical fiber can rotate due to stress-induced birefringence, which changes significantly over time [9]. Temperature, mechanical stress, and other factors also affect operation. The result is that although fiber lasers based on NPE modelocking can operate over periods of months without manual adjustment, during this period substantial drift in operation of the laser is evident, culminating in the laser failing to modelock.

Here we show that liquid crystal (LC) phase retarders provide an attractive method for electrical control of NPE. LC retarders require low drive voltages, their response time is short, and they have good stability over time. While the damage threshold of LCs (500 W/cm^2 for the LCs used here) is lower than Quartz waveplates, it is sufficient for the intracavity powers typical of fiber oscillators. No damage or degradation has been observed. Past work has shown the use of a single LC to start NPE modelocking in an Erbium fiber laser, where the fiber itself was adjusted to allow single element control [10]. However, this scheme did not allow for compensation of changes in the intrinsic birefringence of the fiber over time or environmental perturbations. An alternate LC based modelocking scheme was demonstrated in which an LC-based polarization controller [11] was used to modelock an Erbium soliton fiber laser by controlling the polarization state for NPE [12]. This approach used arbitrary

Optics EXPRESS

polarization control before the polarizer and a single LC after the polarizer. This allows control of the ellipticity of the launch polarization, but not the linear polarization angle.

Along with the development of electronically controllable lasers, there has been recent interest in applying genetic and evolutionary algorithms to the optimization of the multidimensional nonlinear problem of modelocking erbium soliton lasers [6,7,13]. In these, the modelocked operation was found and optimized based on electronic spectrum (FFT) of the pulse train [7], the optical spectral width and electrical spectrum (to encourage single-pulse operation) [6], or second-harmonic generation power [13].

In this work, we design an LC based control scheme that minimizes the number of free parameters, limiting the required control space while maintaining complete control of the polarization into and out of the fiber. We use a total of four LCs in place of the rotatable fixed retarders used in typical NPE modelocked lasers. We demonstrate the utility of this design by using genetic and hill-climbing algorithms to automatically modelock an all-normal dispersion (ANDi) fiber laser and find the optimum operating point with the desired spectral and pulse characteristics.

2. Theory of operation

Figure 1 shows an example of an ANDi oscillator modelocked using NPE [14]. The laser cavity can be divided into two sections: a section of single mode fiber (both passive and doped non-polarization maintaining fiber) and a free space section. When the light exits the single mode fiber its polarization is modified by a quarter wave plate and half wave plate pair, allowing the arbitrary polarization in the fiber to be converted first into an arbitrary linear polarization by the quarter wave plate, which can then be rotated to an arbitrary angle by the half wave plate. The light then travels through a polarizer, which passes some portion of the light (which will be coupled back into the fiber) and rejects some other portion (which may also serve as the laser output, as shown). The amount of light coupled out of the cavity depends on the angle of the half wave plate.

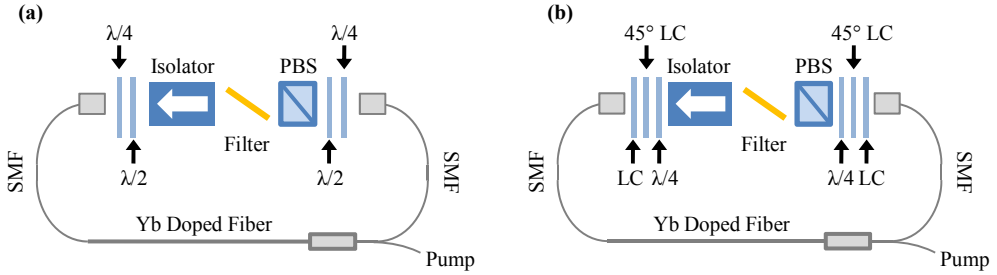

Fig. 1. Schematic of an ANDi laser (a) with and (b) without liquid crystals. The LCs give the ability to fully address all possible polarization states, meaning the laser can be kept in the same state even when the system is greatly perturbed. PBS: Polarizing beam splitter; SMF: Single mode fiber

The transmitted cavity light is spectrally filtered (as required for stable pulse formation in the ANDi laser [15,16]) before transmission through a Faraday isolator to ensure the light only propagates in one direction through the cavity. The output of the Faraday isolator is a linear polarization at 45 degrees. A quarter wave plate then changes the linear polarization into an elliptical polarization where the degree of ellipticity is dependent on the rotation angle of the quarter wave plate. With only a quarter waveplate, as is often used, the systems cannot access the full polarization phase space and therefore, cannot recover similar laser parameters for all environmental and laser drift perturbations. Since the ANDi laser output spectrum and chirp varies significantly with operating point [17], complete control of the polarization is necessary to ensure the laser is returned to the previous operating point. For this reason, a

Optics EXPRESS

second half wave plate can be placed before the quarter wave plate on the output side to allow complete control of the polarization launched into the single mode fiber.

Since the intrinsic and extrinsic stresses in the fiber can change with time and from environmental variations [9], we require that the polarization control at the output of the fiber be capable of converting any polarization state to a linear polarization state at any angle. Likewise, we require that the polarization controller used just before coupling back into fiber be capable of operating on the 45-degree linear polarization (from the isolator) and converting it to an arbitrary polarization state. It has been shown that three liquid crystals can be used to convert from one arbitrary polarization to another arbitrary polarization [11], but this general solution is more complex than is needed in this case. In general, you need a minimum of two degrees of freedom (retardance or rotation angle) in both locations to achieve full control of the polarization in the cavity as described.

Liquid crystal polarization control

To achieve the desired level of control, we use a combination of two LC variable retarders along with a fixed quarter-wave retarder. The two variable retarders (LCs) replace the two rotating waveplates in the standard configuration, with the addition of the quarter-wave plate necessary to allow the LCs to operate in a fixed position (without rotating). In this configuration, there are no mechanical movements required to tune the polarization state. The LCs are oriented such that their fast axes are at 45 degrees relative to one another. A quarter wave plate is placed behind the LCs, with the fast axis oriented parallel to the fast axis of the first LC (placing it also 45 degrees relative to the second LC). This same assembly may be used in reverse, equivalent to switching the positions of the quarter wave plate and the first LC. Both orientations are shown in Fig. 2.

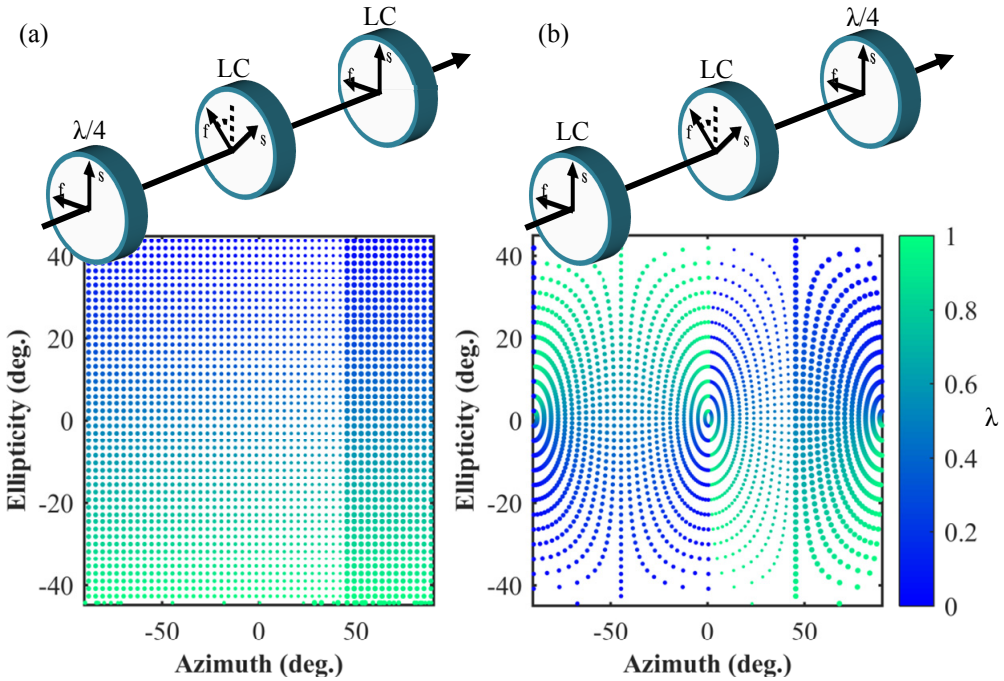

Fig. 2. Diagram of the two configurations of the LC stack showing the (a) forward and (b) backward propagation directions. The simulated output polarizations are shown over the full range of the two LCs for a 45° linear input polarization. The size of the marker indicates the relative magnitude of the first LC, while the color indicates the magnitude of the second LC.

Optics EXPRESS

We can describe the polarization evolution in our liquid crystal based controllers by modeling each element using a Jones matrix, and representing the field with Jones vector. This analysis applies only to polarized light and neglects loss. Considering an input field E, which can be written in the x and y directions can be represented as E_x = cos(α) and E_y = sin(α) exp(i δ), where we have defined a linear polarization angle α and a relative phase between the two polarization components δ, which describes an arbitrary polarization of azimuth α and ellipticity δ. We can then write the output through the LC assembly as

$$E_{out} = J(\lambda/4)\, R(-45°)\, J(\rho_2)\, R(45°)\, J(\rho_1)\, E_{in} \quad (1)$$

where J(η) is the Jones matrix for a retarder with a retardance of η, R(θ) is the rotation matrix for rotation of angle θ, λ is the wavelength of the incident light, and ρ_1 and ρ_2 are the retardance values on the first and second retarders, respectively. It is convenient to convert to the notation of the Stokes parameters, both for concise representation and for comparison to measured values. The first Stokes parameter (S_0) is ignored as it relates to the intensity. The other parameters are normalized and assume the light is completely polarized. The Stokes parameters for the output field can be written as

$$\begin{aligned} S_1 &= \cos(\rho_2)\cos(2\alpha) + \sin(\rho_2)\sin(2\alpha)\sin(\rho_1 - \delta) \\ S_2 &= \sin(\rho_2)\cos(2\alpha) - \cos(\rho_2)\sin(2\alpha)\sin(\rho_1 - \delta). \\ S_3 &= -\cos(\rho_1 - \delta)\sin(2\alpha) \end{aligned} \quad (2)$$

To achieve an arbitrary linear polarization, we require that the ellipticity be zero (and thus need $S_3 = 0$). To achieve this, we can set the first retarder such that ρ1 – δ = (2n + 1) π/2, for any integer n. With this value set, the Stokes parameters become $S_1 = \cos(\rho_2 - 2\alpha)$, $S_2 = \sin(\rho_2 - 2\alpha)$, and $S_3 = 0$. This represents a linear polarization at an angle $\rho_2 - 2\alpha$. To meet our second requirement, we consider a 45° linear polarization (E_x = cos(45°) and E_y = sin(45°)) that we need to transform into an arbitrary polarization. Applying the transformation matrix from the LC stack yields Stokes parameters $S_1 = \sin(\rho_2)$, $S_2 = \cos(\rho_2)\sin(\rho_1)$, and $S_3 = \cos(\rho_2)\cos(\rho_1)$. These equations (which define a sphere of unit radius) are equivalent to the definition of the Poincaré Sphere, the surface of which contains all pure polarization states. This demonstrates the ability of this design to convert a 45° linear polarization to an arbitrary polarization. It can also be shown this conversion to arbitrary from arbitrary linear using this configuration; a 45° input polarization was demonstrated here as the input polarization in this case is known because of the cavity design.

This system gives the desired control over the polarization state as long as the range of the retarders is at least 2π. Using a retarder with a limited range will render some polarizations non-accessible. Similarly, angular misalignment of the elements within the cell will cause incomplete control over the polarization state.

Automation and optimization

With the polarization state in the laser cavity electronically controllable, we want to eliminate manual searching and optimization of the modelocking, and allow an algorithm to test a variety of states and optimize the mode locking of the laser. To achieve this, we define a measure of the fitness of the laser state. This measure can include whether the laser is modelocked, the shape of the spectrum or spectral similarity to previous spectra, the output power of the laser, or the transform-limited pulse duration of the measured spectrum. We use different fitness functions during initial searching for modelocked states and optimization of the laser to a previous good state.

For initial modelocking, we are primarily measuring that the laser is outputting a pulse train, as opposed to CW output. We measure a portion of the laser output with a fast photodiode, filter the photodiode signal with an electronic bandpass filter centered at the

Optics EXPRESS

expected repetition rate of the laser (based on the cavity design), and measure the RF power through this filter. By comparing the RF power to a variable threshold, we can differentiate between CW and modelocked operation. Q-switched operation is also eliminated by probing the RF power multiple times in a row. The spectrum of the modelocked laser can be measured once the laser is determined to be modelocked, and the measured spectrum accepted or rejected based upon metrics set by the user. Many hundreds or thousands of modelocked states can be found in this way.

In the case of laser optimization, in which we are attempting to compensate for perturbations or drift of the system and return the laser to a known-good operating point, we define a metric to gauge the similarity between the current and desired (reference) laser state. In the case of an ANDi laser, a good metric is the spectral similarity combined with the output power. For spectral similarity, we use the coefficient of determination, R^2 [18], although other spectral overlap metrics could be used. The fractional change in output power vs the reference power, $(P - P_{ref})/P$, where P is the optical power of the laser and P_{ref} is the reference optical power, can be linearly combined with the R^2 value to create the fitness function.

Now that we have control over the laser cavity and a defined fitness function, we turn to the process of optimization. The high dimensionality of the search space (roughly $1.5x10^{11}$ points for 10 mrad resolution in phase on each actuator) makes exhaustive testing of every possible state of the laser prohibitively time consuming. Thus, we can turn to preexisting metaheuristics for optimization. A multitude of generic optimization algorithms could be applied to this problem, including iterative local methods like gradient descent or hill climbing, global methods like simulated annealing [19] or threshold accepting [20], or population-based heuristics like evolutionary algorithms [21]. Such algorithms can also be used in conjunction with one another, for example a memetic algorithm in which a local optimization strategy is applied to each member of a population-based algorithm during optimization.

3. Results and discussion

We constructed LC assemblies as described above, and replaced the waveplates in an ANDi fiber oscillator, as shown in Fig. 1(b). The LCs (Meadowlark Optics) and waveplates (Tower Optical) are glued into a machined aluminum housing and placed at the input and output of the fiber section. The other free-space components include a polarizing beam splitter (Precision Photonics), which serves as the output coupler, a birefringent plate that serves as the spectral filter, and an isolator (EO Tech) to enforce a single propagation direction. The fiber cavity consists of two short lengths of single-mode fiber to couple in and out of the cavity, a pump combiner, and a section of Yb-doped double-clad gain fiber. The fiber length is chosen to provide 13 dB absorption of the 976-nm pump light. The multimode pump diode is running at approximately 2 W. This combination of components gives a nominal repetition rate of 59.5 MHz. The output power varies for different states of the laser in the range of 400 – 650 mW.

We can then begin by taking a sparse random or grid-based sampling of the four-dimensional control space, which can be accomplished in a matter of minutes, hours, or days (depending on the desired density of points), and provides some insight into the type of algorithm that may be useful in optimizing the modelocked state.

Optics EXPRESS

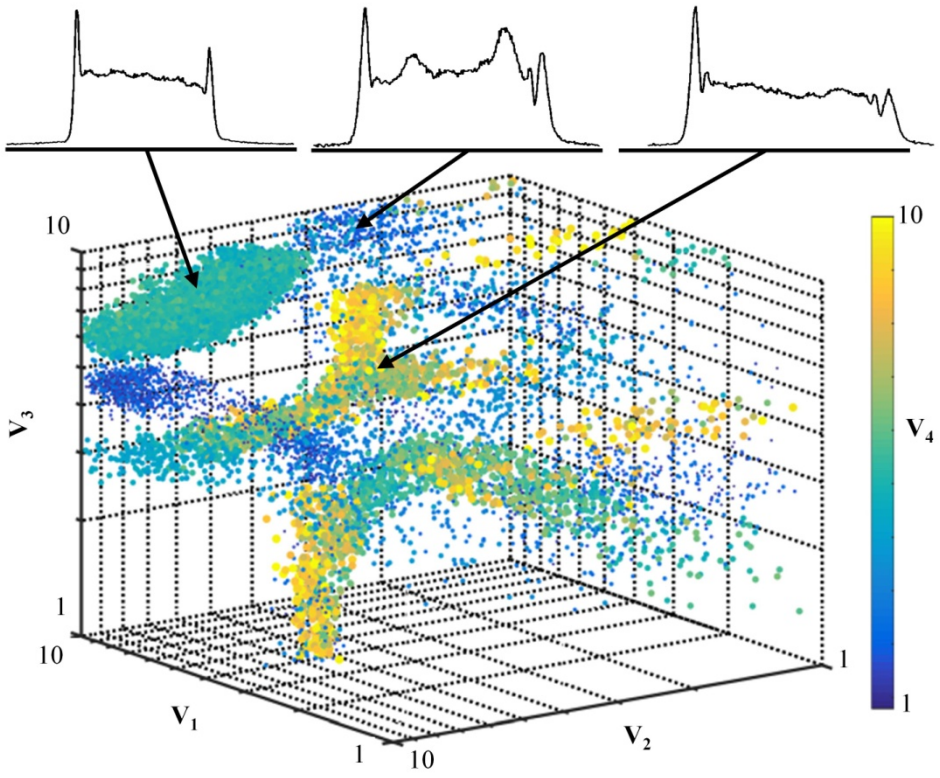

Fig. 3. States found through a scan over all available voltages, showing spectra for several operating points. Three of the four control values are represented as spatial dimensions, with the fourth value represented by the color and diameter of the marker.

Figure 3 shows the results of such a scan, in which 1,000,000 randomly generated control vectors are tested over the course of 17 hours, yielding roughly 22,000 modelocked states. From these data, those states which show evidence of CW breakthrough or incomplete modelocking are rejected. Typically, CW breakthrough appears as a sharp spike roughly centered within the ANDi spectrum. Such spectra can be rejected by looking for large discontinuities in the spectrum between the characteristic bat-ears by calculating the gradient of the spectrum in this region. CW breakthrough can also appear as a distinct peak, usually appearing to the red side of the spectrum, as the filter used in this work is sinusoidal. These spectra can be rejected by computing the integrated signal above 1065 nm and requiring it to be a small fraction of the signal from 1030 nm – 1065 nm, the main wavelength band of interest. The control voltages corresponding to the remaining 8900 states are shown in the scatter plot. As can be seen, there exist multiple discontinuous “clouds”, each corresponding to a modelocked region of operation. The ideal optimization algorithm must thus be capable not only of optimizing for a local maximum, but perform both local and global optimization.

To demonstrate modelocking using a global optimization algorithm, we implement a genetic algorithm. The genetic algorithm creates a random population of some number N control vectors and checks their fitness. The solutions are ranked, and new solutions are generated through mutation (random changes to control values) and/or crossover (swapping of control values) from the population. These new ‘child’ control vectors are generated from a pair of ‘parent’ vectors. The parents are randomly chosen, with the probability of selecting each parent proportional to the rank of that solution. In this way, any vector could be chosen to breed, but higher-ranked solutions breed more often. We also require the two parent

Optics EXPRESS

vectors to be distinct. The values of the control vector are serialized into a single string of numbers to prepare for the next operations.

The two parents are then used to create children through the process of crossover. A random number is compared to the crossover probability, a user-set parameter, to determine if crossover will occur. If selected, a second random number is generated to select which part of the control vector will be swapped between the two solutions. The next operation is mutation. In mutation, each digit in the control series has a probability of being replaced with a random number, with the probability controlled by the 'mutation rate'. The initial rate is set by the user, and can also be bounded by the user, but varies based on the value of the fitness function. This variability prevents the population from becoming too uniform by increasing the mutation rate if fitness values are too clustered, and encourages convergence by decreasing the mutation rate if the fitness spread becomes too large. Once both operations have been completed, the child states will be inserted into the population in place of the two lowest ranked states. The ranks are then recalculated, and the process begins again with selection of new parents. The algorithm terminates after a fixed number of runs, or when the desired fitness is achieved.

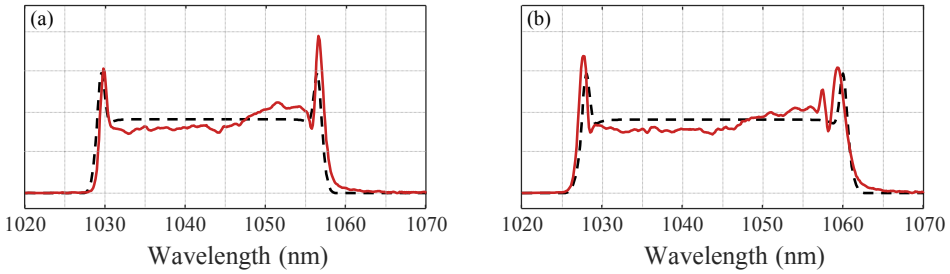

Fig. 4. Spectrum found by GA targeting an idealized ANDi spectrum defined by a center wavelength of 1043 nm and width of (a) 25 nm and (b) 32 nm. The target spectrum and measured spectra are both normalized to their integrated count, and displayed in normalized units. Both spectra are compensated for the responsivity of the array detector.

The GA can now be used to modelock the laser. The R^2 fitness function requires a target spectrum, which can be a desired operating point, an idealized spectrum, or a measured spectrum from previously built ANDi laser with desirable characteristics. To demonstrate this capability, we generate two idealized ANDi spectra, both centered at 1043 nm, the center wavelength of the filter in the cavity. We define the two idealized spectra to have widths of 25 nm and 32 nm FWHM, respectively. Each is used as the target spectrum in the fitness function, in turn. The population size is set to 50, and the algorithm allowed to run for up to 20 generations. The crossover probability is fixed at 25%, with the mutation rate starting at 0.25 and allowed to vary as a function of the fitness. The GA finds spectra which match quite well the desired spectral shape (having R^2 of 0.94 and 0.95, respectively), as shown in Fig. 4. It converged to these solutions in 12 and 19 generations, respectively. These results are a single run of the genetic algorithm; further optimization is possible using the local search. This demonstrates the capability to find spectra that meet the user's general parameter requirements. The fitness function could be modified to allow optimization of other parameters, such as shortest transform-limited duration.

To demonstrate the ability of the GA to find recover a previous operating state, we use as the reference spectrum a previously measured spectrum from this laser. Figure 5(c) shows the spectrum found the GA, with the fitness again calculated as the R^2 of the measured spectrum (solid) and the target spectrum (dashed). The algorithm converged to this solution in 9 generations using a population size of 50 in approximately 90 seconds. The mutation rate was allowed to vary based on the value of the fitness function, again starting at 0.25, and the crossover probability was fixed at 25%.

Optics EXPRESS

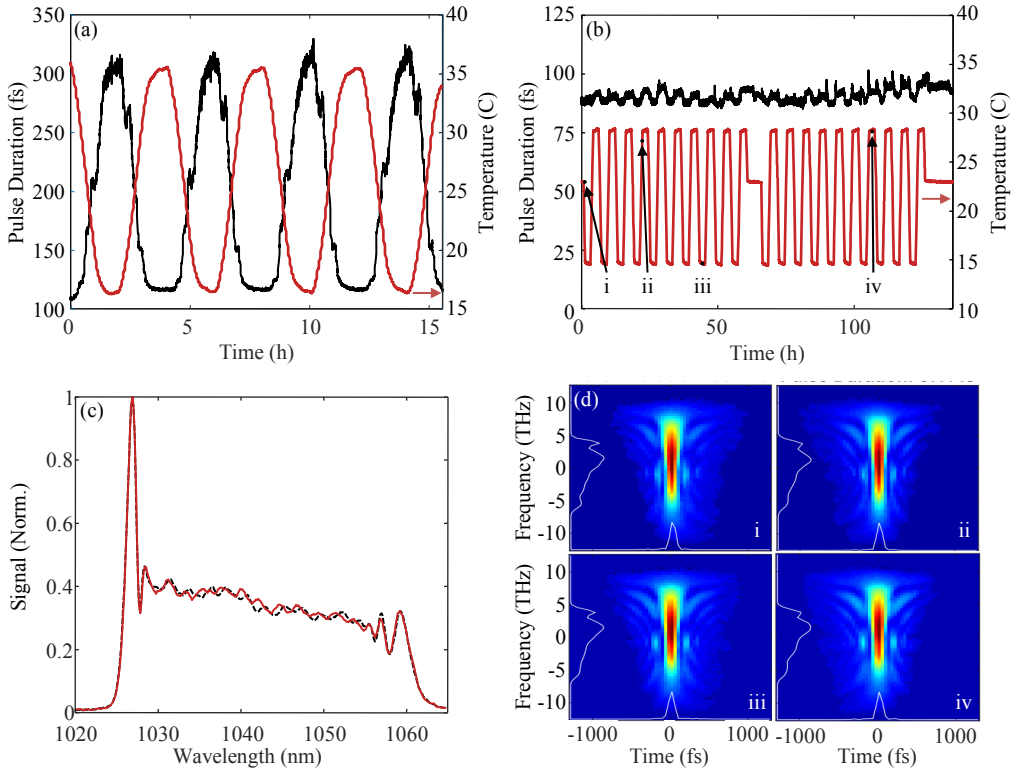

Fig. 5. Pulse duration as a function of environmental temperature in (a) a standard oscillator and (b) a LC stabilized oscillator (minimizing spectral error and power error). (c) Spectrum of the LC mode-locked ANDi laser (solid) recovered by GA from a random starting point using a target spectrum (dashed). (d) Measured FROG traces taken during the temperature cycling run, with the numbers i-iv corresponding to the time and temperatures indicated in (b). The spectral and temporal traces are inset in white along the appropriate axes.

Global optimization is useful when the current state of the laser is far from the target, or when a broad search is otherwise desirable. In many cases, the laser is operating near the desired point, and the solution can be found quickly using a local search algorithm. A simple example of such a local search is hill climbing. In this search, a perturbation is randomly generated for each of the four controls and added to the current control values. Each perturbation is a uniformly-distributed random number selected in a magnitude range of -width to width, where the width is a user-set parameter. Typical values are in the range of 0.005 for fine optimization to 0.05 for more broad exploration, where 1 is a full wave of retardance. The perturbations, in both the hill climber and genetic algorithm, are done in retardance space as the LC retardance is non-linear in voltage. The new state is then tested for fitness. If the fitness increases, the modified control values become the new set point; if the new fitness is lower, the system returns to the previous state. The state is then perturbed again, and the algorithm continues again for a fixed number of iterations, or until the desired fitness is reached. Such an algorithm runs in less than 30 seconds.

It is also possible to run such a local search in an ongoing fashion. In this case, the modelocked laser runs without intervention from the algorithm until the fitness, which is being constantly monitored, drops below a user defined threshold. The hill climbing algorithm will then begin. The algorithm runs for a set number of iterations, or until the error drops back below a threshold. This threshold can either be the same as the threshold that caused the algorithm to begin, or can be higher (leaving some dead space to avoid frequent switching of the algorithm on and off).

Optics EXPRESS

Using this method, the laser can be maintained in a specific operating state. To demonstrate this, we vary the environmental temperature first of a standard fiber laser. This change in temperature causes the laser operating point to change—in an ANDi laser, the intrinsic chip of the pulse as well as the shape of the spectrum will change, and both these affect the pulse duration after compression of the chirp using a grating pair. The grating compressor is set to minimize pulse duration at the beginning of the temperature cycling. This results in a very significant variation in pulse duration (measured using FROG) as seen in Fig. 5(a). We then repeat this test with the LC modelocked laser, with the algorithm set to correct the operating point based on the R^2 of the spectrum with respect to the reference spectrum, taken at the beginning of the temperature cycling. The pulse duration, shown in Fig. 5(b), has an RMS deviation of 2.2 fs with average pulse duration of 90 fs. A selection of SHG FROG traces taken during this temperature cycling are shown in Fig. 5(d).

We also tested the ability of the system to compensate for other types of cavity perturbations. In one test, a cavity fiber was displaced by approximately 4 cm, which changed the compressed pulse duration by 30%, from 117 fs to 155 fs, due to the change in operating point. Running the hill climber algorithm yielded a 118-fs pulse of similarly high quality to the initial pulse. In a second test, the fiber was stressed by placing a 50-g stainless steel weight on one of the cavity fibers. Again, this change in stress caused a change in the output pulse, increasing the duration from 117 fs to 213 fs. Running the hill climbing algorithm again recovers a pulse extremely close to the original pulse, with a duration of 119 fs and nearly identical FROG trace.

In summary, we have demonstrated a system for electronic control of NPE modelocking in a fiber laser using 4 LC controls. The design presented minimizes the number of necessary controls, limiting the search space and reducing cost, while still providing complete control of the system. We demonstrated algorithmic modelocking of the laser using both a global search from a random starting point, as well as local searching and optimization of the laser against environmental and cavity perturbations. We also showed the ability to optimize to a specific operating point by comparison to a reference spectrum, as opposed to optimizing for broadest bandwidth or highest power. This is especially relevant in the ANDi laser, as the laser is capable of producing a wide variety of spectra under different conditions. The automation of initial modelocking decreases build time by eliminating manual searching. The automated optimization against environmental perturbations demonstrates a method for overcoming a limitation of NPE modelocked oscillators, while maintaining their advantages.

Funding

Colorado Advance Industries Grant (POGG1 2016-0767)

Acknowledgments

Portions of this work were presented at Nonlinear Optics in 2017, “Electronic Control of Nonlinear Polarization Evolution Modelocking in a Fiber Laser”. Portions of this work have been disclosed in the patent application PCT/US2017/035863.